Sampling reactive regions in phase space by following the minimum dynamic path

Oliver T. Unke, Sebastian Brickel and Markus Meuwly

View Online

Export Citation

CrossMark

ARTICLES YOU MAY BE INTERESTED IN

Sampling reactive regions in phase space by following the minimum dynamic path

View Online   Export Citation   CrossMark

Oliver T. Unke,[a] [iD] Sebastian Brickel, [iD] and Markus Meuwly[a] [iD]

AFFILIATIONS

Department of Chemistry, University of Basel, Klingelbergstrasse 80, CH-4056 Basel, Switzerland

[a]Authors to whom correspondence should be addressed: oliver.unke@unibas.ch and m.meuwly@unibas.ch

ABSTRACT

Understanding mechanistic aspects of reactivity lies at the heart of chemistry. Once the potential energy surface (PES) for a system of interest is known, reactions can be studied by computational means. While the minimum energy path (MEP) between two minima of the PES can give some insight into the topological changes required for a reaction to occur, it lacks dynamical information and is an unrealistic depiction of the reactive process. For a more realistic view, molecular dynamics (MD) simulations are required. However, this usually involves generating thousands of trajectories in order to sample a few reactive events and is therefore much more computationally expensive than calculating the MEP. In this work, it is shown that a "minimum dynamic path" (MDP) can be constructed, which, contrary to the MEP, provides insight into the reaction dynamics. It is shown that the underlying concepts can be extended to directly sample reactive regions in phase space. The sampling method and the MDP are demonstrated on the well-known 2-dimensional Müller-Brown PES and for a realistic 12-dimensional reactive PES for sulfurochloridic acid, a proxy molecule used to study vibrationally induced photodissociation of sulfuric acid.

Published under license by AIP Publishing. https://doi.org/10.1063/1.5082885

I. INTRODUCTION

Understanding the mechanistic details of a reaction is one of the central goals of chemistry. In particular, one aim is to identify "active" degrees of freedom, which correspond to internal motions promoting the reaction to occur. Once such modes are identified, they can be used to answer questions such as: (i) which initial conditions lead to a reaction within a given time to reaction t_r or (ii) how likely is a reaction to occur from a given set of initial conditions?

Knowledge of the active modes could even be exploited to drive a reaction forward, which is the aim of (coherent) control in chemistry.[1,2] Given the advances in laser technology, it is now possible to deposit energy selectively in specific internal degrees of freedom and to follow redistribution of this energy.[3,4] Controlling chemical reactions in such a way is already possible for specific systems at low temperatures (T < 1 K).[5] Unfortunately, identifying the degrees of freedom relevant for a reaction is not an easy task.[6,7]

Chemical reactions are driven by the underlying, multidimensional potential energy surface (PES). Once the (reactive) PES for a system is known, its topography and the dynamics on it can be studied by computational means. Starting from two minima on the PES (e.g., reactant and product states), it is a common practice to construct the so-called minimum energy path (MEP) connecting them, for example, using the nudged elastic band (NEB) method.[8] A modified algorithm, the climbing image nudged elastic band (CINEB)[9] method also allows to find the transition state (TS) connecting both minima. Alternatively, a method like conjugate peak refinement[10] could be used to locate the TS. However, the MEP is merely a convenient mathematical construct to connect reactant and product states and has little relevance for the dynamics on the PES.[11] While the MEP can provide insight into the overall reaction mechanism, it hides important features pertaining to the reaction dynamics, such as the participating internal or active degrees of freedom and how energy flows between them.

In order to construct a realistic dynamical path, different approaches can be followed. For example, it is possible to formulate the task of finding a path connecting a reactant and product state as a two-point boundary value problem.[12] Such

an approach has been formulated successfully in terms of a minimization problem involving the Onsager-Machlup (OM) action (which requires second derivatives)[13] or a modified target function Θ, that serves as an approximation to the OM action (involving first derivatives only[14]), for which the trajectory is expanded in a Fourier series, known from Fourier path integral simulations.[15] The OM action can be thought of as a measure for the violation of Newton's equations of motion: Every Newtonian trajectory has an OM action of exactly zero. However, starting from arbitrary boundary values, paths determined by minimizing the OM action were found to not necessarily conserve energy, whereas the Θ trajectories do, but are quite similar to a MEP for the Müller-Brown PES.[14]

Alternatively, molecular dynamics (MD) simulations based on accurate energy functions can be used to gain insight into dynamical processes governing a reaction.[16-21] However, for a realistic description of a chemical reaction, a statistically significant number (10^4 or more) of such simulations is required. This is usually not possible with the most accurate approach which would be *ab initio* MD simulations at a sufficiently high level of theory. Therefore, energy functions fitted to electronic structure calculations at a relatively high level of theory (multireference CI for triatomic systems[22] or Møller-Plesset perturbation theory for larger molecules[23,24]) have been used in the past. Running such a large number of MD trajectories is, however, computationally considerably more expensive than calculating the MEP.

For this reason, computational methods were devised to improve the sampling of such rare events. For example, in transition path sampling (TPS), once the dynamical bottleneck of a reaction–its transition state surface–is identified, reactive trajectories can be generated efficiently using Monte Carlo sampling.[25,26] Another example is milestoning, which aims to compute the time scale of complex processes with predetermined "milestones" (slices of the transition path, which are sampled with short trajectories) along a reaction coordinate.[27] Other methods to sample rare events are, for example, the minimum action method,[28] or the string method,[29] which is based on transition path theory.[30] Reaction rates can also be estimated from methods such as transition interface sampling,[31] transition state theory, and extensions thereof,[32-35] which estimate the reactive flux through a so-called dividing surface.

In the present work, the concept of a "minimum dynamic path" (MDP) is considered as an alternative approach and related to the underlying structure of phase space. The MDP corresponds to the lowest energy dynamical (following Newton's equations of motion) reactive path in phase space. Contrary to the MEP, it provides insight into the reaction dynamics and has, by definition, an OM action of zero. Once the transition state of a reaction is known, the MDP can be readily constructed with a computational effort comparable to running a single trajectory (requiring only one additional evaluation of the Hessian). The construction method can easily be extended to generate reactive initial conditions for a microcanonical ensemble of trajectories with arbitrary excess energy ΔE. It is further shown that insights obtained from the MDP are also relevant for reactive trajectories at higher energy.

First, these concepts are investigated for the well-known 2-dimensional Müller-Brown PES[36] for which exhaustive sampling is possible and serves as a validation of the results from the MDP. It is found that particular initial conditions can be prepared which lead to crossing the transition state with certainty. In a next step, the reactive dynamics for a realistic, 12-dimensional reactive PES describing the dissociation dynamics of sulfurochloridic acid[23] is investigated. This molecule is a proxy to study vibrationally induced photodissociation of sulfuric acid.[37,38]

II. THE MINIMUM DYNAMIC PATH AND SAMPLING REACTIVE INITIAL CONDITIONS

Since the transition state of a PES is defined as the configuration $\mathbf{x}_{TS}$ with the highest potential energy $V(\mathbf{x}_{TS}) = E_{TS}$

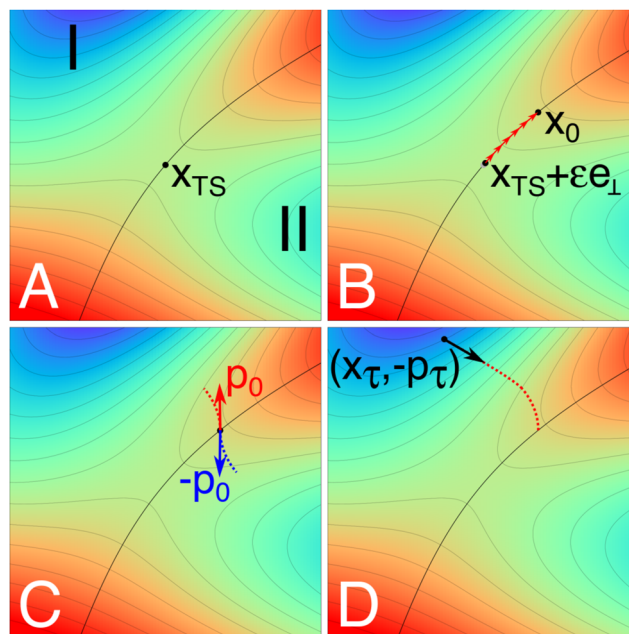**FIG. 1**. Schematic representation of the sampling procedure to generate reactive initial conditions with arbitrary energy $E_{tot} > E_{TS}$. The topology of the potential energy surface is indicated by contour lines and colours, with red tints signifying high energy regions and blue tints low energy regions. (A) The position of the transition state is $\mathbf{x}_{TS}$, I and II label the basins of attraction of the respective minima and the solid black line indicates the separating hypersurface that must be crossed by every trajectory in order to react. (B) Starting from $\mathbf{x}_{TS} + \epsilon \mathbf{e}_\perp$, the direction of steepest ascent (red arrows) is followed until the desired potential energy $V(\mathbf{x}_0) = E_{pot} \leq E_{tot}$ is reached at $\mathbf{x}_0$. Note that the small displacement $\epsilon \mathbf{e}_\perp$ from $\mathbf{x}_{TS}$ is necessary, because at the TS, the direction of steepest ascent is undefined. (C) A momentum vector $\mathbf{p}_0$ with random direction is drawn from a uniform distribution and scaled such that $E_{kin} + E_{pot} = E_{tot}$. Two short trajectories (indicated by dotted lines) are started from the initial conditions $(\mathbf{x}_0, \mathbf{p}_0)$ (red) and $(\mathbf{x}_0, -\mathbf{p}_0)$ (blue) in order to confirm that both trajectories evolve towards different basins of attraction. If not, a new combination $(\mathbf{x}_0, \mathbf{p}_0)$ is generated. (D) Either of the trajectories is followed up to time τ and its final state $(\mathbf{x}_\tau, \mathbf{p}_\tau)$ is recorded. Due to time reversal symmetry, a trajectory starting from $(\mathbf{x}_\tau, -\mathbf{p}_\tau)$ will pass the separating hypersurface after time τ and is therefore reactive.

along the minimum energy path (MEP), every reactive trajectory with constant energy must have a total energy $E_{tot} = E_{pot} + E_{kin} \geq E_{TS}$. Consequently the reactive trajectory with the lowest possible total energy $E_{tot} = E_{TS}$ must pass through the TS exactly and have a kinetic energy $E_{kin} = 0$ at the TS. The path this special trajectory follows through configurational space will henceforth be referred to as the minimum dynamic path (MDP). Note that the MDP and the MEP differ because a dynamical system is not only guided by forces, i.e., the gradient of the PES (which solely determines the MEP), but also keeps a "memory" of past gradients in its current momenta. In the over-damped limit, this memory is completely lost and trajectories approach the MEP (see also Sec. S1).

Transition states are mathematically defined as first-order saddle points of the potential energy surface $V(\mathbf{x})$, i.e., saddle points at which the Hessian has only one negative eigenvalue λ_n with corresponding eigenvector $\mathbf{e}_n$. The MDP can be readily approximated by starting two trajectories at the TS with initial momenta $\mathbf{p}_0 = \pm\epsilon\mathbf{e}_n$ (where ϵ is small) and following their paths through phase space until the desired reactant or product state of the reaction is reached. Since the equations of motion are symmetric under time reversal, both paths can be combined to give the MDP.

It is also possible to extend this procedure to generate reactive initial conditions $(\mathbf{x}, \mathbf{p})$ in phase space with $E_{tot} \geq E_{TS}$.

For this, the concept of a "separating hypersurface" is introduced: Consider a PES with two minima labelled I and II and a saddle point TS separating them. Starting at an arbitrary point P in configuration space and following the direction of steepest descent, every path initiated at P will reach either I, II, or rarely the TS. The sets of points that converge to I or II form the basin of attraction for the respective minima, whereas the set of points that converges to TS forms a hypersurface separating those basins of attraction [see Figs. 1 and 2(A)]. This hypersurface must be crossed by every reactive trajectory going from I to II at some point and is referred to as the separating hypersurface. Note that points on this hypersurface do not react equally likely to either I or II, i.e., this surface differs from the isocommittor surface.[6,7,39] It is also distinct from the concept of a dividing surface used in TPS. The dividing surface is the hypersurface with the lowest number of recrossings for which trajectories reach educt and product states equally likely.[26] The topology of the separating hypersurface on the other hand does not contain any dynamic information and depends solely on the underlying PES. It is important to point out that while the sampling method presented here does generate reactive initial conditions, they do not correspond to a thermal ensemble. In the limit of infinite sampling, rates from a microcanonical and a canonical treatment are identical though, even for a few-particle system.[40]
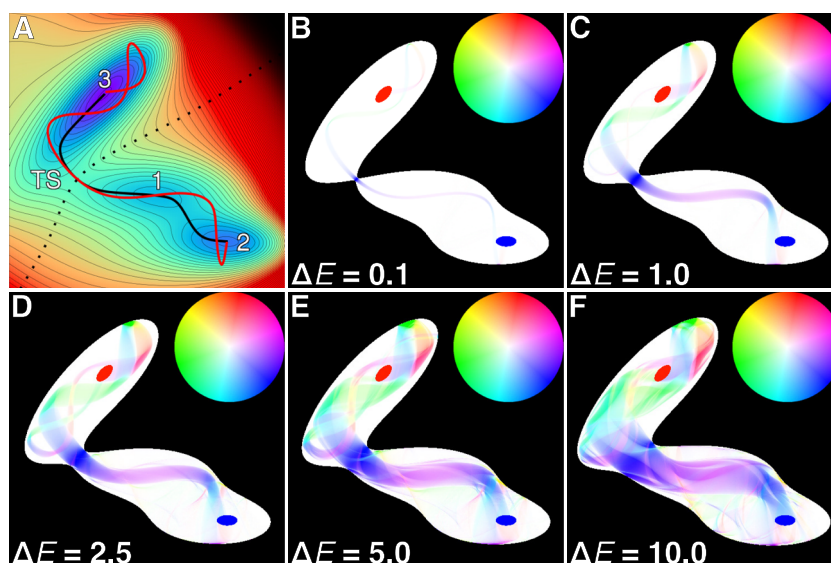

FIG. 2. (A) Topology of the Müller-Brown PES.[36] Contour lines are drawn every 10 energy units starting at $E = -145$. The minima marked with 1, 2, and 3 correspond to energies of $E_1 \approx -80.768$, $E_2 \approx -108.167$, and $E_3 \approx -146.700$, respectively, whereas the TS is at $E_{TS} \approx -40.665$. The solid black and red lines depict the minimum energy path (MEP) and the minimum dynamic path (MDP) of a particle with mass $m = 1$ between minima 2 and 3, respectively. The dotted black line indicates the separating hypersurface between the basins of attraction of minima 1 and 2 and minimum 3. Panels (B)–(F): Depiction of the subspace of phase space with constant energy $E = E_{TS} + \Delta E$ for trajectories of a particle with mass $m = 1$ that evolve from the reactant state (red ellipsis) to the product state (blue ellipsis) in time $t \leq 20$. Black regions are energetically inaccessible. The colours encode the average direction of reactive trajectories in momentum space for a given point in coordinate space according to the colour legend shown in the top right corner of each panel. More saturated colours indicate a stronger preference for a particular direction in momentum space, whereas completely white regions contain no reactive trajectories at all. For small ΔE, the overall shape of the reactive part of phase space closely resembles the MDP (see the solid red line in panel A). For large ΔE, alternative "reaction channels" become accessible, but pathways resembling the MDP remain dominant. Both, exhaustive unbiased sampling and the procedure described in Sec. II converge to the same reactive subspace [shown as coloured regions in panels (B)–(F)]. See Fig. S1 for a variant of this figure with oversaturated colours that increase visibility of reaction channels.

To sample a reactive initial condition $(\mathbf{x}, \mathbf{p})$ in phase space with energy $E_{tot} \geq E_{TS}$, these steps are followed:

1. A point $\mathbf{x}_0$ with potential energy $E_{pot} \leq E_{tot}$ is generated on the separating hypersurface as follows: Starting at configuration $\mathbf{x} = \mathbf{x}_{TS} + \epsilon \mathbf{e}_\perp$ [see Fig. 1(A)], where $\mathbf{x}_{TS}$ is the configuration of the TS, ϵ is a small number and $\mathbf{e}_\perp$ is a random direction perpendicular to $\mathbf{e}_n$, the gradient is followed along the direction of steepest ascent until the desired energy E_{pot} is reached at point $\mathbf{x}_0$ [see Fig. 1(B)]. The small initial displacement by $\epsilon \mathbf{e}_\perp$ is required because at the transition state, the direction of steepest ascent is undefined. Following the gradient ensures that the point $\mathbf{x}_0$ lies on the separating hypersurface, which generally is curved.

2. A momentum vector $\mathbf{p}_0$ with random direction is drawn from an unbiased distribution and its magnitude scaled such that $E_{tot} = E_{kin} + E_{pot}$. It should be noted that drawing momenta from an unbiased distribution and scaling their magnitude generates reactive initial conditions corresponding to a microcanonical ensemble. In order to obtain thermal reactive initial conditions, the momenta would have to be drawn from a flux-weighted distribution.[41]

3. A trajectory is started with initial conditions $(\mathbf{x}_0, \pm \mathbf{p}_0)$. A short MD simulation with both initial conditions [Fig. 1(C)] is necessary in order to verify that the two trajectories move towards the two different basins of attraction, which is not guaranteed *a priori*.

4. If this requirement is met, a longer trajectory is run until time τ (which is chosen arbitrarily) starting from either $(\mathbf{x}_0, \mathbf{p}_0)$ or $(\mathbf{x}_0, -\mathbf{p}_0)$ and the final positions and momenta $(\mathbf{x}_\tau, \mathbf{p}_\tau)$ are recorded [Fig. 1(D)]. Since the equations of motion are time reversal symmetric, a trajectory starting from the initial condition $(\mathbf{x}_\tau, -\mathbf{p}_\tau)$ is reactive and will pass the separating hypersurface after the chosen time τ. All reactive trajectories generated in this fashion form the "reactive phase space," i.e., a subset of productive initial conditions which lead to the reaction (cross the separating hypersurface). Note that this sampling procedure is conceptually similar to "shooting" in TPS,[42] but here, trajectories are always started on the separating hypersurface instead of a point in configurational space reached after a random time.

III. THE MDP FOR THE MÜLLER-BROWN SURFACE

In order to verify that the procedure described in Sec. II can be applied and used to extract information about the underlying dynamics, the well-known 2-dimensional Müller-Brown PES[36] is considered

$$V(x, y) = \sum_{i=1}^{4} A_i e^{a_i(x-x_{0,i})^2 + b_i(x-x_{0,i})(y-y_{0,i}) + c_i(y-y_{0,i})^2} \qquad (1)$$

with $A = [-200, -100, -170, 15]$, $a = [-1, -1, -6.5, 0.7]$, $b = [0, 0, 11, 0.6]$, $c = [-10, -10, -6.5, 0.7]$, $x_0 = [1, 0, -0.5, -1]$, and $y_0 = [0, 0.5, 1.5, 1]$. The PES features three minima of increasing depth with energies $E_1 \approx -80.768$, $E_2 \approx -108.167$, and $E_3 \approx -146.700$. The

transition state (TS) connecting the deepest minimum with the shallower minima corresponds to an energy of approximately $E_{TS} \approx -40.665$ [see Fig. 2(A)].

Since the phase space corresponding to the Müller-Brown system is only 4-dimensional $((x, y, p_x, p_y))$, it is possible to determine all regions in phase space that lead to reaction by exhaustive sampling. In order to test whether the method described in Sec. II samples the same regions as such an unbiased sampling, an unambiguous definition of a reactive trajectory is required. For this purpose, the trajectory of a particle with mass $m = 1$ and total energy $E_{tot} = E_{TS} + \Delta E$ is considered to be reactive if it reaches minimum 2 (product state) within time $t_{max} = 20$ starting from minimum 3 (reactant state). A trajectory is terminated when it reaches the product state within $t \leq t_{max}$ in which case it is "reactive" or after t_{max} in which case it counts as "unreactive", even if it could react at a later time. Reactant and product states are defined to be the set of points (x, y) enclosed by ellipses centered around the corresponding minima given by the parametric equations

$$x(s) = x_0 + \frac{1}{10} \cos(s) \cos(\phi) - \frac{1}{20} \sin(s) \sin(\phi),$$
$$y(s) = y_0 + \frac{1}{20} \sin(s) \cos(\phi) + \frac{1}{10} \cos(s) \sin(\phi) \qquad (2)$$

with $x_0 \approx -0.56$, $y_0 \approx 1.44$, and $\phi = \pi/4$ defining the reactant state and $x_0 \approx 0.62$, $y_0 \approx 0.028$ and $\phi = 0$ defining the product state [see blue and red ellipses in Figs. 2(B)–2(F)]. These definitions are largely arbitrary, but needed in order to define unambiguous reactant and product states. The equivalence between exhaustive unbiased sampling and the method described in Sec. II can be tested with any arbitrary definition of states and choice of t_{max}.

The reactive part of phase space is sampled exhaustively by generating trajectories with unbiased random initial conditions (x, y, p_x, p_y) such that the total energy corresponds to $E_{tot} = E_{pot} + E_{kin} = E_T + \Delta E$. If a trajectory starting from (x, y, p_x, p_y) reaches the product state in time t_1 and a trajectory starting from $(x, y, -p_x, -p_y)$ reaches the reactant state in time t_2 such that $t_1 + t_2 \leq t_{max}$, the initial condition (x, y, p_x, p_y) belongs to the reactive part of the phase space [see Figs. 2(B)–2(F)]. Note that with increasing excess energy ΔE, more states on the separating hypersurface become energetically accessible, which leads to a widening of the transition region, which is also known from explicit reactive MD simulations.[43] Furthermore, while the MDP remains representative for most of the reactive part of phase space, with increasing excess energy additional "reaction channels" open up [see Figs. 2(B)–2(F)] for which the time until the product state is reached can differ significantly (see Fig. S2). It is interesting to note that, depending on ΔE, the tubes emanating from either A or B do not cover the entire boundary of the ellipses but rather correspond to discrete regions in phase space (see Fig. S1).

In summary, the method described in Sec. II is able to efficiently sample the reactive regions in phase space and converges to the same set of initial conditions as unbiased sampling (see Fig. 2). This is also the reason why the results from explicit sampling are not reported separately. Comparing the

reactive part of phase space (even for large excess energy ΔE) with the MDP also shows that the MDP is representative for the reactive phase space explicitly sampled by the system; see, e.g., Figs. 2(A) and 2 (C).

It should be noted that a decomposition of phase space into reactive and non-reactive subspaces has been observed in earlier work and is even possible in the absence of an imposed maximum reaction time t_{max} due to the presence of trapped orbits.[44]

IV. APPLICATION TO MOLECULAR SYSTEMS: SULFUROCHLORIDIC ACID

In order to study the MDP for a concrete *molecular* system, the dissociation of sulfurochloridic acid (HSO_3Cl) into HCl and SO_3 is considered for which a fully, 12-dimensional reactive PES,[23] constructed with the MS-ARMD method,[18] is available. The transition state for the $HSO_3Cl \rightarrow SO_3 + HCl$ dissociation reaction lies at $E_{TS} \approx 31.5$ kcal/mol above the energy minimum. Both, MEP and MDP for the reaction were constructed. Because phase space is now much higher dimensional than for the Müller-Brown surface, it is not possible to compare MEP and MDP by a simple projection onto the PES. To still be able to highlight differences, the evolution

of the distance d of the sulfur atom to the plane defined by the three oxygen atoms (pyramidalization), as well as the distance between sulfur and chlorine atom r_{S-Cl}, is considered along with molecular structures sampled at a fixed interval (snapshots of the trajectories), see Fig. 3.

While both MEP and MDP display comparable overall movement, the MEP lacks important dynamical information: In the MDP, the SO_3 moiety oscillates between a pyramidal and a planar arrangement, which suggests that this "umbrella motion" plays a key role in the reaction (see d and r_{S-Cl} in Fig. 3). While it would be possible to guess the importance of this mode from the MEP alone, the MDP reveals the order and time scale when different modes become active prior to the reaction and when they mix with other modes. This is particularly relevant in the context of ultracold and controlled chemistry: For example, conformer-specific reactions have been investigated where, depending on the conformer and the activating mode considered, the coupling to the remaining degrees of freedom changes and therefore the reaction outcome depends on how and how much energy is deposited in the system.[45] As such, the MDP provides time-resolved information into the energetics and structural dynamics prior to the reaction when approaching the transition state. For example, the MDP in Fig. 3(a) reveals
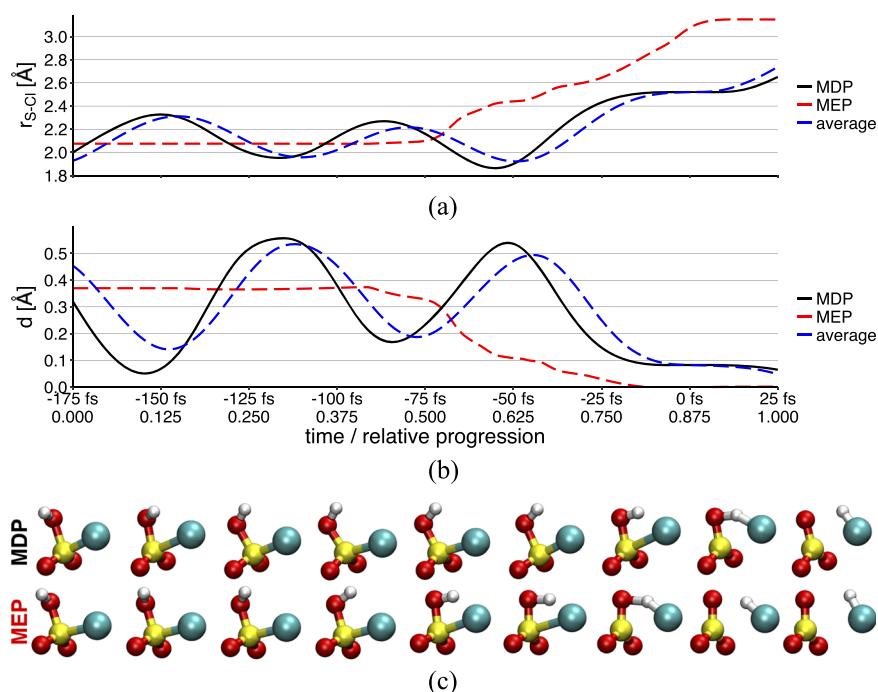

FIG. 3. Evolution of distance r_{S-Cl} of sulfur and chlorine atom (a) and distance d of the sulfur atom to the plane defined by the three oxygen atoms (b) for the minimum dynamic path (MDP, solid black line), averaged over 100 trajectories with excess energy $\Delta E = 5$ kcal/mol above the saddle point (average, dashed blue line) and minimum energy path (MEP, dashed red line). This excess is an illustrative value but is also close to the zero-point energy of the OH stretch vibration. For the MDP and the averaged results, the point in time at which the trajectory crosses the separating hypersurface is set to zero and the time relative to the crossing point is indicated. For the MEP, the notion of time is meaningless and relative progression from the start point (0.000) to the end point (1.000) is indicated instead. The MEP lacks important dynamical features that promote the reaction, e.g., the oscillation of the SO_3 moiety between a pyramidal ($d > 0$) and a planar ($d = 0$) structure. See also the snapshots depicting the overall motion for both paths (c, top row: MDP; bottom row: MEP; sampled at the intervals given on the x-axis). Note that on average, reactive trajectories follow a motion comparable to the MDP. However, the oscillation period of d (and r_{S-Cl}) is shortened due to increased kinetic energy.

that the S–Cl bond (solid black for MDP and dashed blue for average over 100 reactive trajectories) breaks at a later point in time during the reaction than the MEP would suggest (dashed red). In this example, the MEP evidently only provides time-averaged information, whereas the MDP provides insights on how relevant modes communicate; i.e., the MDP is sensitive to the underlying couplings as the system approaches the transition state. Consider, for example, the pyramidalization d: Between the progression coordinate 0.0–0.5, the value of d in the MDP oscillates around an average value of 0.29 ± 0.25 Å, whereas reactive trajectories oscillate on average around a mean value of 0.33 ± 0.20 Å. In the MEP on the other hand, d remains constant at ~0.37 Å. Similar observations can be made for the Müller-Brown PES, where the MDP oscillates around the MEP [see Fig. 2(A)]. Such dynamics occurs on a time scale (sub-picosecond) that should be amenable to state-of-the art, controlled experiments.[46]
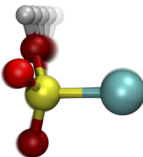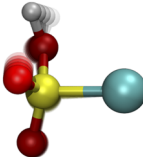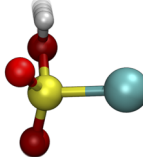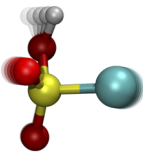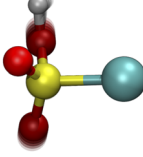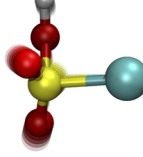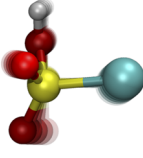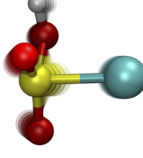
In order to verify that the umbrella motion−found to be an important degree of freedom in the MDP−is also relevant in reactive trajectories with excess energy, 100 initial conditions that lead to dissociation within 175 fs were run with an excess energy of $\Delta E = 5$ kcal/mol; see Sec. II. MD simulations using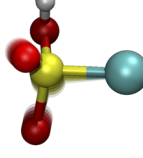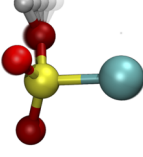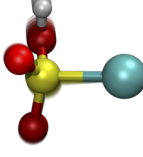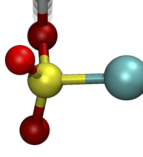 a custom code were run with the velocity Verlet integrator[47] and a time step of 0.1 fs for a total of 2000 time steps. All these trajectories follow a similar motion compared to the MDP prior to the elimination reaction (see Fig. 3): Averaging all reactive trajectories exhibits the same oscillatory behaviour as observed for the MDP. For short time-scales (~0.2 ps) prior to the reaction, it appears that reactive trajectories all exhibit a similar "concerted" motion, at least for this particular case, and that this coupling can be visualized and analyzed. Of course, the details of this observation depend on the underlying PES.

For quantifying key aspects of the underlying motion, the total energy of the MDP trajectory and the 100 reactive trajectories is decomposed into normal mode[48] contributions. Table I reports the harmonic frequencies ω of all 12 normal modes corresponding to internal degrees of freedom together with their associated motion.

The normal mode decomposition analysis is performed as follows: Given Cartesian coordinates $\mathbf{x}$ and corresponding momenta $\mathbf{p}$ for a specific snapshot, first, $\mathbf{x}$ and $\mathbf{p}$ are transformed to the Eckart frame,[49] which removes translational and rotational contributions. Next, the potential and kinetic energies are separately projected onto normal modes. For the potential energy, the normal mode coordinates $\mathbf{q}$ are calculated from $\mathbf{x}$. Then, for every normal mode i a new coordinate

TABLE I. Normal modes of HSO_3Cl in energetically ascending order. The first 6 normal modes correspond to translational and rotational motions and are omitted. The corresponding atomic displacements for each normal mode are shown as motion trace (H: white, O: red, Cl: cyan, S: yellow) and normal mode frequencies for the optimized structure on the MS-ARMD PES[23] are reported.

No.	Motion	ω (cm^{-1})	No.	Motion	ω (cm^{-1})	No.	Motion	ω (cm^{-1})
7		258	11		510	15		1143
8		317	12		523	16		1176
9		325	13		555	17		1407
10		384	14		814	18		3773

vector $\tilde{\mathbf{q}}^i$ is generated, where all entries $\tilde{q}^i_{j \neq i}$ are set to the equilibrium values and $\tilde{q}^i_i$ corresponds to the ith entry of $\mathbf{q}$. Finally, $\tilde{\mathbf{q}}^i$ is transformed back to Cartesian coordinates $\tilde{\mathbf{x}}^i$ to obtain the contribution of the potential energy along a specific normal mode i. The potential energy E^i_{pot} of normal mode i is then defined as

$$E^i_{\text{pot}} = \frac{E_{\text{pot}}(\tilde{\mathbf{x}}^i)}{\sum_i E_{\text{pot}}(\tilde{\mathbf{x}}^i)} E_{\text{pot}}(\mathbf{x}) \tag{3}$$

which ensures that the true potential energy $E_{\text{pot}}(\mathbf{x})$ of configuration $\mathbf{x}$ is divided exactly among the normal modes, such that $\sum_i E^i_{\text{pot}} = E_{\text{pot}}(\mathbf{x})$.

For the kinetic energy, the velocities $\mathbf{v}$ derived from the momenta $\mathbf{p}$ are transformed to a vector $\mathbf{w}$ in normal mode space in the same way $\mathbf{x}$ is transformed to $\mathbf{q}$. Note that due to the way the transformation into normal modes is defined, the entries w_i of $\mathbf{w}$ correspond to the "momentum" of each normal mode i divided by the square root of the associated effective mass. The kinetic energy E^i_{kin} of normal mode i is defined accordingly as

$$E^i_{\text{kin}} = \frac{w_i^2}{\sum_i w_i^2} E_{\text{kin}}(\mathbf{p}), \tag{4}$$

where $E_{\text{kin}}(\mathbf{p})$ is the true kinetic energy according to the momenta $\mathbf{p}$, which ensures that it is divided exactly among the normal modes.

The total energy of a normal mode is then simply the sum of its kinetic and potential energy. It should be noted that the method described above does not guarantee $E_{\text{tot}} = \sum_i E^i_{\text{kin}} + E^i_{\text{pot}}$ because of rovibrational coupling, which leads to some vibrational energy being unaccounted for in the transformation to the Eckart frame. Nonetheless, the total energy is conserved approximately and will fluctuate around a constant mean with a typical amplitude of <0.1 kcal/mol, which is sufficient for the present purpose. Also, it should be noted that the normal mode decomposition assumes a harmonic PES and is thus only strictly valid close to the equilibrium geometry. When the normal mode decomposition is performed in highly anharmonic regions, results can get distorted and should therefore always be considered with care. Still, the decomposition provides a quantitative comparison of the relative importance of normal modes between different trajectories. Note that other methods to decompose the energy into normal mode contributions are possible.[50,51]

Figure 4 shows the normal mode energy decomposition for different times prior to the reaction for the MDP and an average for an ensemble of 100 reactive trajectories. While the MDP and the ensemble statistics differ slightly, they both follow qualitatively similar trends. Furthermore, the analysis confirms that mode 13, which corresponds to an "umbrella motion" of the SO_3 moiety, and mode 18, which corresponds to the OH stretch vibration, are excited prior to the reaction, a trend which could already be deducted from a visual inspection of the MDP. Thus, the molecular picture that arises from this analysis suggests that energy flows from other degrees of freedom into these modes, which promote dissociation. This
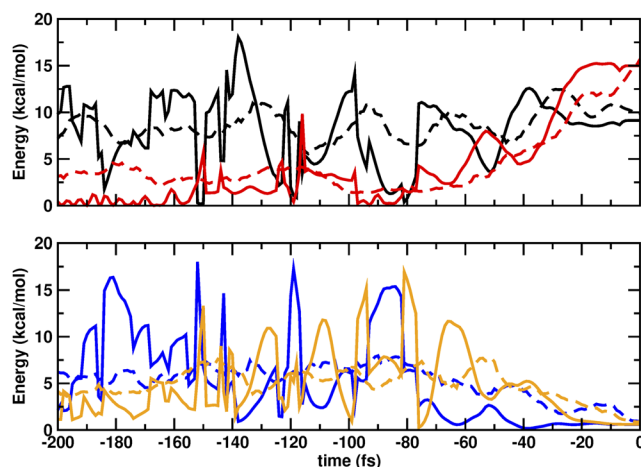

FIG. 4. Normal mode decomposition analysis of the total (kinetic and potential) energy for reactive trajectories for HSO_3Cl. For clarity, only the four modes with the highest fluctuations are shown: (top panel) modes 13 (black) and 18 (red), and (bottom panel) modes 14 (blue) and 16 (orange). Modes 14 and 16 are the SOH bend and the SO stretch modes, respectively. Trajectories reach the separating hypersurface at $t = 0$ fs. Solid lines indicate the results for the minimum dynamic path (MDP), whereas dashed lines are averaged over 100 trajectories with a total energy corresponding to $\Delta E = 5$ kcal/mol above the transition state energy. Around $t = -175$ fs, modes 13 and 14 carry more energy than other modes. Some of this energy is transferred to mode 16 during the next 100 fs. Between -75 fs and -50 fs before the reaction, modes 14 and 16 start to lose energy, whereas mode 18 becomes excited. Around $t = -30$ fs, modes 13 and 18 contain by far the largest fraction of the total energy (33% and 30% for the MDP, 34% and 20% for the averaged results). Note that while it is difficult to directly correlate time points between MDP and the averaged results due to a difference in kinetic energy of up to $\Delta E = 5$ kcal/mol, both results show similar trends and the dynamics of the energy flow between modes is comparable.

is consistent with a previous study which demonstrated that vibrationally induced photodissociation can be promoted via vibrational energy redistribution by exciting the -OH stretching motion.[23]

V. REACTIVE TRAJECTORIES VERSUS VIBRATIONAL ENERGY RELAXATION

In order to test whether the insights about the reaction dynamics gathered from analysis of the MDP are applicable in a more general context, the differences between non-reactive and dissociative trajectories of HSO_3Cl after OH-stretch overtone excitation were studied using the normal mode decomposition scheme described earlier. The reactive MD simulations (with the exception of using the velocity Verlet integrator[47]), were carried out along the same lines as in the previous study.[23] The change of the integrator was necessary to allow a meaningful normal mode energy decomposition analysis.

Individual trajectories were started from a geometry optimized structure of HSO_3Cl. The system was heated to 300 K. The equations of motion were propagated using the leapfrog Verlet algorithm with a time step of $\Delta t = 0.1$ fs during 50 ps and equilibrated for 50 ps, followed by 50 ps of free dynamics simulations.
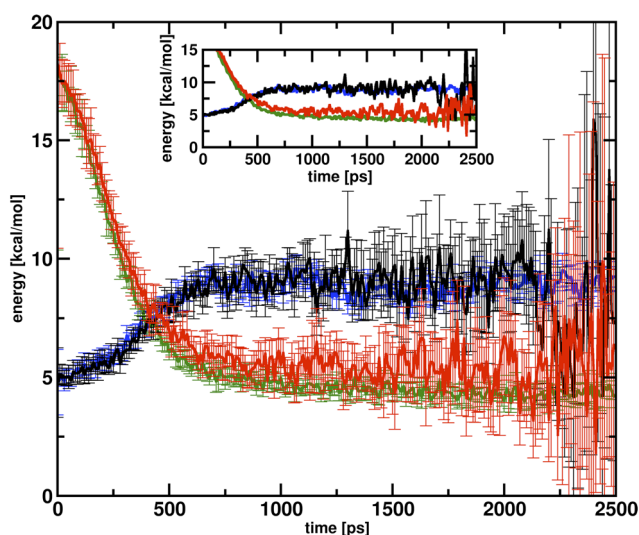
FIG. 5. Average energy analysis for modes 13 (black—reactive; blue— nonreactive) and 18 (red—reactive; green— nonreactive) for 205 dissociative and 364 non-reactive HSO_3Cl trajectories after OH-stretch excitation.

Because the previous study indicated that the reaction time is on the nanosecond time scale when five quanta of OH stretch are excited, the reactive MD simulations were run with the corresponding excitation energy of 50.5 kcal/mol.[23] A total of 764 simulations were run with a time step of $\Delta t = 0.1$ fs for a maximum simulation time of 2.5 ns. Of those, a total of 205 directly dissociating trajectories (HCl elimination without prior H-transfer[23]), and 364 non-reactive trajectories (no HCl elimination and no H-transfer within 2.5 ns of simulation time), were analysed. For both of these sets of trajectories, the total energy was decomposed following the normal mode procedures outlined above.

Figure 5 shows the average normal mode energy for modes 13 and 18 for reactive and non-reactive trajectories including fluctuations. The energy content and flow within and between these modes does not differ for the two classes of trajectories when ensemble averages and fluctuations around them are considered. Hence, contrary to the dynamics on the Müller-Brown PES the initial conditions do not decompose phase space into two types of trajectories that could be distinguished after initial preparation (here vibrational excitation), at least when energy content in the participating modes is used to differentiate between them. This is consistent with the intuitive notion that the fate of a trajectory− whether it leads to reaction or not−is decided in the phase immediately before bond breaking occurs; see also Fig. 4. The reason for this is most likely the high dimensionality of phase space which leads to mixed, chaotic dynamics (the Lyapnuov time[52] for this system was determined to lie between 2 and 5 ps).

VI. CONCLUSION

The concept of an MDP was introduced, which is related to the MEP but includes dynamical effects due to inertia. It was shown that the MDP resembles the dynamics of an ensemble of reactive trajectories, thus providing valuable insight into the reaction dynamics of a system of interest with a single trajectory. Furthermore, a method was described which allows direct sampling of reactive phase space, making the generation of reactive initial conditions for MD simulations more efficient. The techniques were demonstrated for the 2-dimensional Müller-Brown model system and a more realistic 12-dimensional reactive PES for sulfurochloridic acid. Conclusions drawn from the MDP about which modes promote dissociation in HSO_3Cl also hold for OH-stretch overtone induced photodissociation, which was confirmed by energy decomposition analysis for reactive and non-reactive trajectories of HSO_3Cl.

The techniques discussed here can also be applied to *ab initio* molecular dynamics simulations in the gas phase. Because for an initial assessment of a particular reactive trajectory between a given reactant and product state only one MDP simulation is required, it will be possible to use high-level electronic structure theory methods (MP2 or even CCSD(T) depending on system size) to obtain information about the participating degrees of freedom. Similarly, applications to condensed phase systems, e.g., to investigate competitive ligand rebinding[53] or bimolecular reactions in solution[54] should be possible to determine relevant degrees of freedom accompanying the reaction. Once such active degrees of freedom are known, they could be used to drive a chemical system by controlled excitation of the corresponding motions.

SUPPLEMENTARY MATERIAL

See supplementary material for additional figures. This material is available free of charge via the Internet at http://pubs.acs.org/.

REFERENCES

[1] R. Gordon, L. Zhu, and T. Seideman, Acc. Chem. Res. **32**, 1007–1016 (1999).
[2] L. Levin, W. Skomorowski, L. Rybak, R. Kosloff, C. P. Koch, and Z. Amitay, Phys. Rev. Lett. **114**, 233003 (2015).
[3] A. H. Zewail, J. Phys. Chem. A **104**, 5660–5694 (2000).
[4] W. S. Warren, H. Rabitz, and M. Dahleh, Science **259**, 1581–1589 (1993).
[5] R. V. Krems, Phys. Chem. Chem. Phys. **10**, 4079–4092 (2008).
[6] A. Ma and A. R. Dinner, J. Phys. Chem. B **109**, 6769–6779 (2005).
[7] R. B. Best and G. Hummer, Proc. Natl. Acad. Sci. U. S. A. **102**, 6732–6737 (2005).
[8] H. Jónsson, G. Mills, and K. W. Jacobsen, *Classical and Quantum Dynamics in Condensed Phase Simulations* (World Scientific, 1998), pp. 385–404.
[9] G. Henkelman, B. P. Uberuaga, and H. Jónsson, J. Chem. Phys. **113**, 9901–9904 (2000).
[10] S. Fischer and M. Karplus, Chem. Phys. Lett. **194**, 252–261 (1992).

[11] P. Pechukas, J. Chem. Phys. **64**, 1516–1521 (1976).

[12] R. Elber and M. Karplus, Chem. Phys. Lett. **139**, 375–380 (1987).

[13] R. Olender and R. Elber, J. Chem. Phys. **105**, 9299–9315 (1996).

[14] D. Passerone and M. Parrinello, Phys. Rev. Lett. **87**, 108302 (2001).

[15] J. D. Doll, D. L. Freeman, and T. L. Beck, Adv. Chem. Phys. **78**, 61–127 (1990).

[16] M. Meuwly, Wiley Interdiscip. Rev.: Comput. Mol. Sci. **9**, e1386 (2018).

[17] S. C. L. Kamerlin and A. Warshel, Faraday Discuss. **145**, 71–106 (2010).

[18] T. Nagy, J. Yosa Reyes, and M. Meuwly, J. Chem. Theory Comput. **10**, 1366–1375 (2014).

[19] B. K. Carpenter, J. N. Harvey, and D. R. Glowacki, Phys. Chem. Chem. Phys. **17**, 8372–8381 (2015).

[20] O. T. Unke and M. Meuwly, J. Chem. Inf. Model. **57**, 1923–1931 (2017).

[21] C. Qu, Q. Yu, and J. M. Bowman, Annu. Rev. Phys. Chem. **69**, 151–175 (2018).

[22] O. Denis-Alpizar, R. J. Bemish, and M. Meuwly, Phys. Chem. Chem. Phys. **19**, 2392–2401 (2017).

[23] J. Yosa Reyes, S. Brickel, O. T. Unke, T. Nagy, and M. Meuwly, Phys. Chem. Chem. Phys. **18**, 6780–6788 (2016).

[24] S. Brickel and M. Meuwly, J. Phys. Chem. A **121**, 5079–5087 (2017).

[25] C. Dellago, P. G. Bolhuis, F. S. Csajka, and D. Chandler, J. Chem. Phys. **108**, 1964–1977 (1998).

[26] P. G. Bolhuis, D. Chandler, C. Dellago, and P. L. Geissler, Annu. Rev. Phys. Chem. **53**, 291–318 (2002).

[27] A. K. Faradjian and R. Elber, J. Chem. Phys. **120**, 10880–10889 (2004).

[28] E. Weinan, W. Ren, and E. Vanden-Eijnden, Commun. Pure Appl. Math. **57**, 637–656 (2004).

[29] E. Weinan, W. Ren, and E. Vanden-Eijnden, Phys. Rev. B **66**, 052301 (2002).

[30] E. Weinan and E. Vanden-Eijnden, J. Stat. Phys. **123**, 503–525 (2006).

[31] D. Moroni, T. S. van Erp, and P. G. Bolhuis, Physica A **340**, 395–401 (2004).

[32] R. Hernandez and W. H. Miller, Chem. Phys. Lett. **214**, 129–136 (1993).

[33] R. Hernandez, J. Chem. Phys. **101**, 9534–9547 (1994).

[34] R. Hernandez, T. Uzer, and T. Bartsch, Chem. Phys. **370**, 270–276 (2010).

[35] O. Sharia and G. Henkelman, New J. Phys. **18**, 013023 (2016).

[36] K. Müller and L. D. Brown, Theor. Chem. Acc. **53**, 75–93 (1979).

[37] Y. Miller and R. B. Gerber, J. Am. Chem. Soc. **128**, 9594–9595 (2006).

[38] J. Yosa Reyes, T. Nagy, and M. Meuwly, Phys. Chem. Chem. Phys. **16**, 18533–18544 (2014).

[39] E. Weinan, W. Ren, and E. Vanden-Eijnden, Chem. Phys. Lett. **413**, 242–247 (2005).

[40] R. M. Stratt and J. E. Adams, J. Chem. Phys. **78**, 2368–2373 (1983).

[41] J. B. Anderson, J. Chem. Phys. **58**, 4684–4692 (1973).

[42] C. Dellago, P. G. Bolhuis, and P. L. Geissler, Adv. Chem. Phys. **123**, 1–78 (2002).

[43] D. R. Nutt and M. Meuwly, Biophys. J. **90**, 1191–1201 (2006).

[44] B. J. Berne, N. De Leon, and R. Rosenberg, J. Phys. Chem. **86**, 2166–2177 (1982).

[45] Y.-P. Chang, K. Długołkecki, J. Küpper, D. Rösch, D. Wild, and S. Willitsch, Science **342**, 98–101 (2013).

[46] N. Balakrishnan, J. Chem. Phys. **145**, 150901 (2016).

[47] L. Verlet, Phys. Rev. **159**, 98 (1967).

[48] E. B. Wilson, J. C. Decius, and P. C. Cross, *Molecular Vibrations: The Theory of Infrared and Raman Vibrational Spectra* (Courier Corporation, 1980).

[49] C. Eckart, Phys. Rev. **47**, 552 (1935).

[50] G. Czako, A. L. Kaledin, and J. M. Bowman, Chem. Phys. Lett. **500**, 217–222 (2010).

[51] B. Jiang and H. Guo, J. Chem. Phys. **138**, 234104 (2013).

[52] B. P. Bezruchko and D. A. Smirnov, *Extracting Knowledge from Time Series: An Introduction to Nonlinear Empirical Modeling* (Springer Science & Business Media, 2010).

[53] K. Nienhaus, S. Lutz, M. Meuwly, and G. U. Nienhaus, Chem. - Eur. J. **19**, 3558–3562 (2013).

[54] C. G. Elles and F. F. Crim, "Connecting chemical dynamics in gases and liquids," Annu. Rev. Phys. Chem. **57**, 273–302 (2006).